Computer Assisted Methods in Engineering and Science, **23**: 191–204, 2016.

An optimal design of micro-drill from the aspect of vibration analysis

Tien-Dat Hoang[1], Danh-Tuyen Nguyen[2], An-Chen Lee[2]
[1] *Faculty of International Training, Thai Nguyen University of Technology Vietnam*
e-mail: hoangdat@tnut.edu.vn
[2] *Department of Mechanical Engineering, National Chiao Tung University Taiwan, R.O.C*

This paper presents an approach to optimize the structure of a micro-drill for reducing its lateral vibration, which has a strong effect on the quality of drilled holes during the cutting process. The micro-drill and the spindle of a micro-drilling spindle system are modeled as Timoshenko's beam elements. Each element with five degrees of freedom at each node comprehensively includes the effects of continuous mass eccentricity, shear deformation, gyroscopic moments, rotational inertia with external thrust force and torque, and coupling torsional and lateral effect. The finite element method is used to determine the lateral amplitude response at the micro-drill point, which is considering the objective function during the optimization of the micro-drill by the interior-point approach. The diameters and the lengths of drill segments are chosen as the design variables with nonlinear constraints in the constant mass, mass center location, and torsional deformation of the drill. The in-house finite element code-integrated optimization environment is implemented in MATLAB to solve the optimal problem. The results showed that compared with the original micro-drill, the lateral amplitude response at the drill point of the optimal one is reduced by 91.89% at an operating speed of 50 000 rounds per minute (r/min), and its first critical speed and the corresponding amplitude response exceed those of the original one.

Keywords: nonlinear constrained optimization, finite element analysis, micro-drilling spindle, continuous eccentricity.

Nomenclature

E, G	–	Young's modulus and shear modulus,
I_u, I_v	–	second moments of area about principle axes U and V of system element,
k_s	–	shear coefficient,
C_{ij}, K_{ij}	–	direct axial damping, stiffness coefficient of the bearing; $i, j = x, y$,
C_φ, K_φ	–	torsional damping and torsional stiffness of the bearing,
F_z, T_q	–	thrust force and torque,
L, A, d, ρ, m	–	length, area, diameter, density, and mass of system element,
N_t, N_r, N_s	–	shape functions of translating, rotational, and shear deformation displacements, respectively,
Z	–	axial distance along system element,
Q	–	DOF vector of the fixed coordinates,
(u, v)	–	components of the displacement in U and V axis coincident with principal axes of system element,
(x, y)	–	components of the displacement in X and Y axes in the fixed coordinates,
t	–	time,
e_u, e_v	–	mass eccentricity components of shaft in U and V axes,

e_x, e_y – mass eccentricity components of shaft in X and Y axes,
θ_u, θ_v – angular displacements about U and V axes, respectively,
θ_x, θ_y – angular displacements about X and Y axes, respectively,
Φ – spin angle between basis axis and X about Z axis,
Ω – rotating speed,
δ, φ – lateral and torsional displacements,
B – the angle between principal axis U and basis axis of the fixed coordinates at the initial angular position.

Subscript

{t} – to be referred to as transpose matrix.

1. Introduction

Engineering of rotating structures is an iterative and multidisciplinary procedure that aims to simultaneously satisfy a wide variety of requirements and constraints. Recently, the improvement of further advances in the technology of rotating machinery, especially in high-speed spindle systems, has played an important role. At a spindle speed of up to 300 000 r/min, the rotation of the systems induces vibrations with different types of oscillations, notably lateral and torsional oscillations. These vibrations may lead to unfavorable noise and unrecoverable failure of cutting tools in high-speed spindle systems. Previously, several studies have been performed on the chatter vibrations of machine tools [3, 6, 11, 12, 14]. To reduce these vibrations, many works have investigated the workpiece, the cutting profile, or the resonant frequency. However, few studies analyzed the behaviors of the cutting tool in a whole spindle system, especially in a micro-drilling spindle system. Moreover, all micro-drilling spindle systems are required to work at higher speeds; as a result, the cutting tool can be easily damaged or even broken. The main aim of this research is to optimize the shape design of a micro-drill bit to reduce its vibration during the cutting process. With the optimal design procedure, the desired micro-drill that satisfies all necessary constraints could be designed and developed first on the computer, so that fewer prototypes have to be made in practice, thereby reducing costs.

Many authors have investigated and optimized, both analytically and experimentally, the dynamic behavior of machine tool spindle-bearing systems. They showed that spindle system dynamics are influenced by a large number of factors, including the holder characteristics [1], spindle shaft geometry, tool shaft geometry, drawbar force [18], stiffness, and damping provided by the bearings [2, 19, 21]. A milling spindle system is presented and implemented in [7]. In [7], the authors performed some optimizations to find the desired rotor location and bearing arrangement to obtain a chatter vibration-free cutting operation at the desired speed and depth of cut for a given cutter. In addition, the significant factors that affect the vibrations of rotor structures were shown through the optimization simulations of structural parameters in [4, 10, 20]. Therefore, a comprehensive study of the rotor shaft with cutting tool should be further conducted by applying vibration optimization in the machining process.

Many optimal methods have been used to optimize rotating systems, such as genetic algorithms [5, 20, 22] and gradient-based methods [15]. A constraint interior-point algorithm, which is a gradient-based algorithm, was applied in a case study of quadratic-programming-based model-predictive rotorcraft control [9]. Similarly, Rao and Mulkay compared the interior-point methods with the well-known simplex-based linear solver in solving large-scale optimum design problems [17]. The interior-point method with suitable numerical algorithms for the mechanical model was applied in this research.

In this paper, the Union MDS micro-drill series tool with a 0.1 mm diameter produced by UNION TOOL Co., a global market leader in the micro-drill industry, is used as a benchmark by applying the nonlinear constrained interior-point algorithm, which is a large-scale algorithm [13]. The optimal

lateral vibration amplitude of the drill point with nonlinear constraints, including constant mass, mass center location, and torsional vibration response constraints, was found by detecting the optimal diameters and the length of each drill segment. The results showed that compared with the original micro-drill, the lateral amplitude at the steady state of the drill point of the optimal one is reduced by 91.89% at an operating speed of 50 000 r/min, and the first critical speed of the optimal micro-drill exceeds the required operating speed.

2. Finite element model of the micro-drilling spindle system

In this paper, the model and its parameters are derived from our previous work as shown in Figs. 1 and 2 [13]. Figure 1 illustrates the schematic system that was used to model a micro-drilling spindle system. The system is divided into four main parts, i.e., spindle A, shaft B, clamps C and D, and the

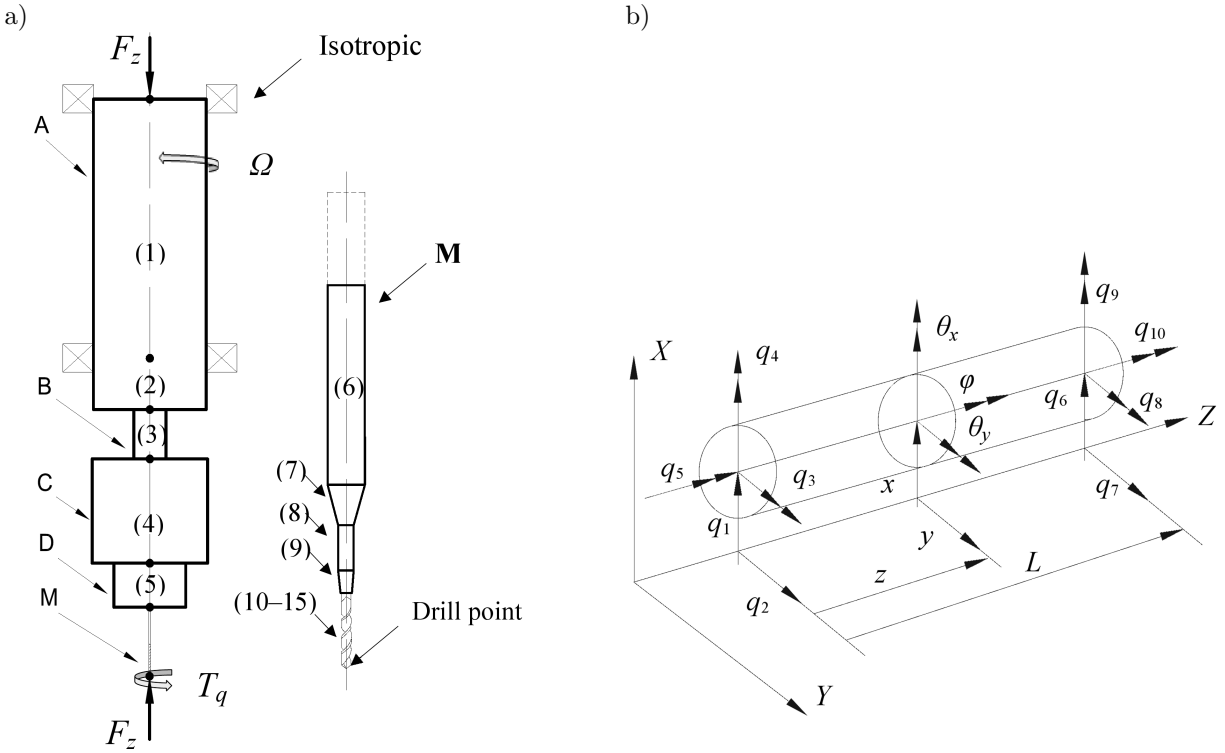

Fig. 1. Finite element model of the micro-drilling spindle: a) model of the micro-drill system, b) five degrees of freedom Timoshenko model.

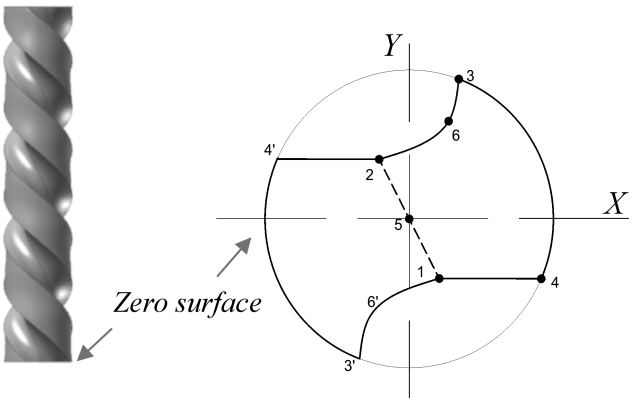

Fig. 2. Cross-section model of the drill tool.

Union MDS drill M. The dimensions and parameters of the system are shown in Tables 1 and 2. The system is divided into 15 finite elements, and the numbering of the elements is shown in Fig. 1a. The finite element method (FEM) formulation is based on a standard beam element with 10 degrees of freedom as shown in Fig. 1b.

Table 1. Parameters of the finite element model of the micro-drilling spindle system.

Element no.	Parameters						
	Length L [mm]	Diameter d [mm]	E [Pa]	G [Pa]	Density ρ [kg/m^3]	e_u [mm]	e_v [mm]
1	37.5	22	2E+11	0.9E+11	7800	$11 \times e_{u0}$	0
2	11.25	22	2E+11	0.9E+11	7800	$11 \times e_{u0}$	0
3	9	6.3	2E+11	0.9E+11	7800	$3.15 \times e_{u0}$	0
4	19	22.5	2E+11	0.9E+11	7800	$11.25 \times e_{u0}$	0
5	8	14	2E+11	0.9E+11	7800	$7 \times e_{u0}$	0
6	10	3.175	2.1E+11	0.9E+11	7800	$1.585 \times e_{u0}$	0
7	4.105	1*	2E+11	0.9E+11	7800	1**	0
8	6.2	0.8	2E+11	0.9E+11	7800	$0.4 \times e_{u0}$	0
9	1.3	2*	2E+11	0.9E+11	7800	2**	0
10–15	0.25	0.1	5.7E+11	3.7E+11	15000	3*	3**
Isotropic bearing parameters							
Bearing stiffness: $K_{xx} = K_{yy} = 1.7513 \times 10^5$ [N/m]; $K_\varphi = 3 \times 10^3$ [Nm rad^{-1}]							
Bearing damping: $C_{xx} = C_{yy} = 1.7513 \times 10^3$ [Ns/m]; $C_\varphi = 1 \times 10$ [Nm s rad^{-1}]							
Shear coefficient: $k_s = 5/6$							

Note that $e_{u0} = 10^{-5}$ is the eccentricity factor;

1* is $d_7 = 3.175 \times (1 - z/L_7) + 0.8 \times (z/L_7)$;

1** is $e_{u7} = 3.175 \times e_{u0} \times (1 - z/L_7) + 0.8 \times e_{u0} \times (z/L_7)$;

2* is $d_9 = 0.8 \times (1 - z/L_9) + 0.1 \times (z/L_9)$;

2** is $e_{u9} = 0.8 \times e_{u0} \times (1 - z/L_9) + 0.1 \times e_{u0} \times (z/L_9)$;

3* is $e_u^f = x_0^e \cos\beta_e^f - y_0^e \sin\beta_e^f$;

3** is $e_v^f = x_0^e \sin\beta_e^f - y_0^e \cos\beta_e^f$,

where $\beta_e^f = \dfrac{2\pi.z}{p} = \dfrac{2\tan\gamma}{d_f} \cdot z$ (radians, $z > p$); the pitch of helix, $p = \dfrac{\pi d_f}{\tan\gamma}$.

Table 2. Other parameters of the Union MDS drill (elements 10–15).

Name	MDS
Diameter d_f [mm]	0.1
Helix angle γ [°]	30
Web thickness υ [mm]	0.04
Flute/land ratio f	1.5/1.0
Chisel edge angle ψ [°]	62.5
Flute length l_f [mm]	1.5
Total length l_0 [mm]	38.1
Area A [mm^2]	5.22×10^{-3}
Second moments of area about principal axes u, I_u [mm^4]	1.68×10^{-6}
Second moments of area about principal axes v, I_v [mm^4]	3.94×10^{-6}

3. Global motion equation of the system

The bearing characteristics play an important role in the vibration behavior of rotor dynamic system. Therefore, to validate the simulation method, two isotropic journal bearings with constant stiffness and constant damping coefficients were modeled. The global motion equation can be expressed by the following equation [13]:

$$[\mathbf{M}_t]\{\ddot{\mathbf{q}}\} + ([\mathbf{C}] + \Omega[\mathbf{G}_t])\{\dot{\mathbf{q}}\} + [\mathbf{K}_t]\{\mathbf{q}\} = \{\mathbf{F}_t\}, \tag{1}$$

where

$$\{q\} = \begin{bmatrix} x_1 & \theta_{y1} & y_1 & \theta_{x1} & \varphi_1 & \dots & x_n & \theta_{yn} & y_n & \theta_{xn} & \varphi_n \end{bmatrix}'$$

is the vector of global DOF in the fixed coordinates, n is the number of nodes for the finite element system, $[\mathbf{M}_t]$ is the assembled mass matrix, $[\mathbf{K}_t]$ is the assembled stiffness matrix, $[\mathbf{C}]$ is the assembled damping matrix, $[\mathbf{G}_t]$ is the assembled gyroscopic matrix, and $\{\mathbf{F}_t\}$ is the assembled force vector [13].

The element displacement is given by

$$[u^e] = [N^e][q^e],$$

where

$$[q^e] = \begin{bmatrix} x_1^e & \theta_{y1}^e & y_1^e & \theta_{x1}^e & \varphi_1^e & x_2^e & \theta_{y2}^e & y_2^e & \theta_{x2}^e & \varphi_2^e \end{bmatrix}^t,$$

which is the node generalized displacement vector, $[N^e]$ is composed from the shape functions that are given in the Appendix, and $[u^e] = \begin{bmatrix} x^e & \theta_y^e & y^e & \theta_x^e & \varphi^e \end{bmatrix}^t$ is the element displacement vector. The machine is assumed to operate with a constant rotating speed Ω about the z-axis. The deflections, in this study, are assumed to be very small. Therefore, the magnitudes of high-order nonlinear terms, which involve square or multiplication terms, are quite small and can be ignored for simplification of the solution for the system of linear time-varying differential equations.

4. Optimal design results

The vibration minimization problem of the micro-drill during the cutting process is solved in this work. The parameters in Tables 1 and 2 were used to simulate the system for the following numerical example. The vibration responses at the micro-drill point are evaluated by Newmark's method. The parameters used to obtain the responses for improved convergence speed and stability are given by $\alpha = 0.25$, $\varsigma = 0.5$; $\Delta t = 6 \times 10^{-5}$ s, where α and ς are the Newmark parameters, and Δt is the time interval.

4.1. Problem formulation

In general, an optimization is performed to find a set of design parameters $\boldsymbol{x} = (x_1, x_2, \dots, x_n)$ that can in some way be defined as optimal so that the objective function $f(\boldsymbol{x})$ is minimized or maximized, subject to constraints in the form of equality $g_{\text{eq}}(\boldsymbol{x})$, inequality $g_{\text{ieq}}(\boldsymbol{x})$, nonlinear constraints $c(\boldsymbol{x})$, and parameter lower and upper bounds. Specifically, they are stated as follows:

The objective function

$$\text{minimize: } \boldsymbol{f}(\boldsymbol{x}) \tag{2}$$

subject to

$$\text{the constraint equations: } \begin{cases} \boldsymbol{g}_{\text{ep}} = \boldsymbol{A} \cdot \boldsymbol{x} - \boldsymbol{b} \le 0, \\ \boldsymbol{g}_{\text{ieq}} = \boldsymbol{A}_{\text{eq}} \cdot \boldsymbol{x} - \boldsymbol{b}_{\text{eq}} = 0, \\ \boldsymbol{c} = \text{function of } \boldsymbol{x}. \end{cases} \tag{3}$$

The lower and upper bounds for design variables:

$$\boldsymbol{x}_{lb} \leq \boldsymbol{x} \leq \boldsymbol{x}_{ub}, \tag{4}$$

where $\boldsymbol{A}$ and $\boldsymbol{A}_{\text{eq}}$ are matrices, and $\boldsymbol{b}$, $\boldsymbol{b}_{\text{eq}}$, $\boldsymbol{x}_{lb}$ and $\boldsymbol{x}_{ub}$ are vectors.

The interior-point method, which is a gradient formulation in the search process, has been proven to be stable and was used by some authors in [8, 16]. Given its advantages, this method for large-scale algorithms of the function ***Fmincon*** in MATLAB was used in this research. Gradients of the objective with scalar function and nonlinear constraints are finite-differencing approximations. The Hessian matrix is updated by the Broyden-Fletcher-Goldfarb-Shanno formulae. The FEM code and optimization environment are implemented to solve the optimal problem.

The accuracy of drilled holes is significantly affected by the lateral vibration at the drill tip of the micro-drill during the cutting process. Hence, to ensure the accuracy of drilled holes, the lateral vibration should be reduced. In some previous works, to reduce the lateral vibration, the objective functions were based on the natural frequencies [22] or the mass of shafts [15], which easily help the optimal process to converge but cannot directly optimize the lateral vibration. In this research, to focus on the drill tip performance, the objection function of the logarithm function of lateral vibration at the drill tip is employed and described by

$$f_{(x)} = \log_{10}(\delta_{\Omega}), \tag{5}$$

where δ_{Ω} is the lateral vibration amplitude at the drill point at the operating speed Ω.

Many factors affect the vibration at the drill tip, such as the micro-drill structure, machine spindle, and cutting velocity. The micro-drill structure is the main concern in this research. It is created by three key parts, namely, the shank, the flute, and the remaining part that connects to the shank and the flute. The flute size, that is, the diameter and the length, is standard and fixed for a particular application. Thus, the size design of the remaining part of a drill bit is our main concern. This design includes the diameters (x_1, x_2) and the lengths (x_3, x_4, x_5) of the drill segments denoted as vector $\boldsymbol{x}$, as shown in Fig. 3. The lengths of cylindrical and conical

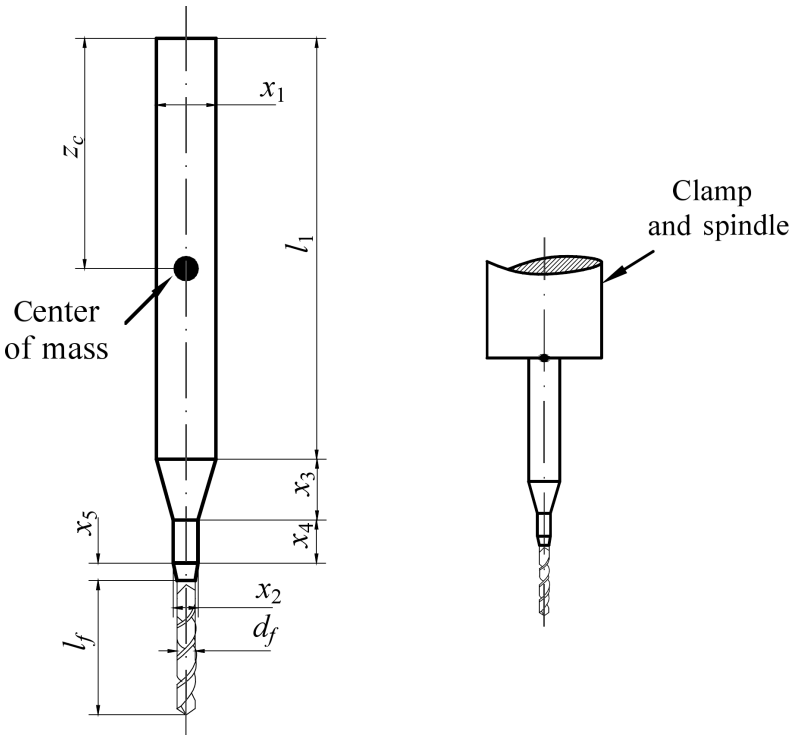

Fig. 3. Schematic of the micro-drill and the clamp.

parts x_3, x_4, x_5 of the micro-drill affect the drill stiffness; longer lengths correspond to lower stiffness. Thus, increasing these lengths will increase the lateral vibration at the drill tip during the cutting process. In addition, an increase in the cross-sectional diameters x_1, x_2 increases the unbalanced force and stiffness. These two factors counteract each other on the lateral displacement. To illustrate this complex optimal design problem with the effect of all variables, a formulation is performed for the MDS drill as shown in Fig. 3 with the original parameters shown in Tables 1 and 2. The system was optimized at the operating speed of 50 000 r/min and $F_z = -2.5$ N, $T_q = 5.5 \times 10^{-3}$ N mm.

The micro-drill length should be constant according to engineering standards. As a result of the geometrical relationship, the cylinder diameter x_2 is smaller than the shank diameter x_1. The mass center location z_c of the drill tool needs to be constrained to ensure that it is inside the tool holder of the machine spindle. The micro-drill mass m is constant. To make the lateral vibration orbit smooth, the deviatoric lateral response percentage $\Delta\delta_{\Omega\%}$ is constrained. To avoid the torsional displacement, φ_Ω is also constrained. All these constraints are presented as follows:

$$\begin{cases} l_f + l_1 + x_3 + x_4 + x_5 - l_0 = 0 & \text{(equality constraint)}, \\ x_2 - x_1 \le 0 & \text{(inequality constraint)}, \\ z_c - z_c^0 \le 0 & \text{(nonlinear constraint)}, \\ m - m_0 = 0 & \text{(nonlinear constraint)}, \\ \Delta\delta_{\Omega\%} - \Delta\delta_{\Omega\%}^0 \le 0 & \text{(percentage error constraint)}, \\ \varphi_\Omega - \varphi_\Omega^0 \le 0 & \text{(percentage error constraint)}, \end{cases} \tag{6}$$

where l_0 is the total length of the original drill, l_f is the flute length of the original drill, z_c^0 is the maximum allowable clamped length of the original drill shank, m_0 is the initial mass of the original drill, $\Delta\delta_\Omega^0\%$ is the maximum allowable of the percentage error, and φ_Ω^0 is the maximum allowable torsional deformation.

The formulae to calculate mass m and mass center location z_c of the drill tool are expressed as

$$m = m_1 + m_2 + m_3 + m_4 + m_f = \rho_1\pi\left(\frac{l_1 \cdot x_1^2}{4} + \frac{x_3 \cdot (x_1^2 + x_2^2 + x_1x_2)}{12}\right) + \rho_2\pi\left(\frac{x_4 \cdot x_2^2}{4} + \frac{x_5 \cdot (x_2^2 + d_f^2 + x_2d_f)}{12}\right) + m_f, \tag{7}$$

$$z_c = \frac{m_1 \cdot z_{c1} + m_2 \cdot z_{c2} + m_3 \cdot z_{c3} + m_4 \cdot z_{c4} + m_f \cdot z_{c5}}{m}, \tag{8}$$

where d_f, m_f, and z_f are the diameter, mass, and mass center location of the flute part, respectively, and the shank length $l_1 = 24.995$ mm as shown in Fig. 3.

$$z_{c1} = \frac{l_1}{2},$$

$$z_{c2} = l_1 + \frac{x_3}{x_1 - x_2}\left(x_1 - \frac{3}{4} \cdot \frac{x_1^4 - x_2^4}{x_1^3 - x_2^3}\right),$$

$$z_{c3} = l_1 + x_3 + \frac{x_4}{2},$$

$$z_{c4} = l_1 + x_3 + x_4 + \frac{x_5}{x_2 - d_f}\left(x_2 - \frac{3}{4}\cdot\frac{x_2^4 - d_f^4}{x_2^3 - d_f^3}\right),$$

$$z_{c5} = l_1 + x_3 + x_4 + x_5 + z_f,$$

$\Delta\delta_{\Omega\%} = \dfrac{\delta_\Omega^{\max} - \delta_\Omega^{\min}}{\delta_\Omega^{\max}} \times 100\%$ is the deviatoric lateral response percentage between the maximum and minimum lateral amplitudes of the response orbit, which significantly affects the drilling quality during steady-state machining at the operating speed Ω [13].

4.2. Numerical example

An optimal numerical example is presented in this section. The bounds and allowable values in the numerical example are chosen as follows:

Table 3. The allowable values of constraint equation.

z_c^0 [mm]	m_0 [g]	$\Delta\delta_{\Omega\%}^0$ [%]	φ_Ω^0 [rad]
15	1.68	5	1.82×10^{-3}

$$\begin{aligned} &0.1 \text{ (mm)} \le x_1, x_2 \le 5 \text{ (mm)}, \\ &0.1 \text{ (mm)} \le x_3, x_4, x_5 \le 10 \text{ (mm)}. \end{aligned} \tag{9}$$

The history of the objective function value during iteration is shown in Fig. 4. After 61 iterations and 473 function evaluations, the optimal process stops when the size of the current step is less than the selected step size tolerance and the constraints are satisfied. The original and optimal response orbits of the model are shown in Figs. 5 and 6. The values of the design variables and constraints that correspond to the original, starting, and optimal points are shown in Table 4.

Table 4. Comparison of the optimal and original results.

		Original value	Starting value	Optimal value	Percentage error between optimal and original value [%]
Design variable	x_1 [mm]	3.175	3.175	3.1946	0.62 (increase)
	x_2 [mm]	0.8	0.8	0.988	23.5 (increase)
	x_3 [mm]	4.105	4.505	1.217	70.35 (decrease)
	x_4 [mm]	6.2	2.1	8.999	45.14 (increase)
	x_5 [mm]	1.3	5	1.389	6.8 (increase)
Nonlinear constraint	z_c [mm]	14.8	14.6	13.85	6.42 (decrease)
	$\Delta\delta_\Omega$ [%]	2.6	2.5	2.8	7.69 (increase)
	δ_Ω [m]	8.33×10^{-9}	3.2×10^{-8}	6.756×10^{-10}	91.89 (decrease)
	$\text{Log}(\delta_\Omega)$	−8.08	−7.5	−9.17	13.5 (decrease)
	φ_Ω [rad]	1.82×10^{-3}	2.5×10^{-3}	0.28×10^{-3}	85 (decrease)

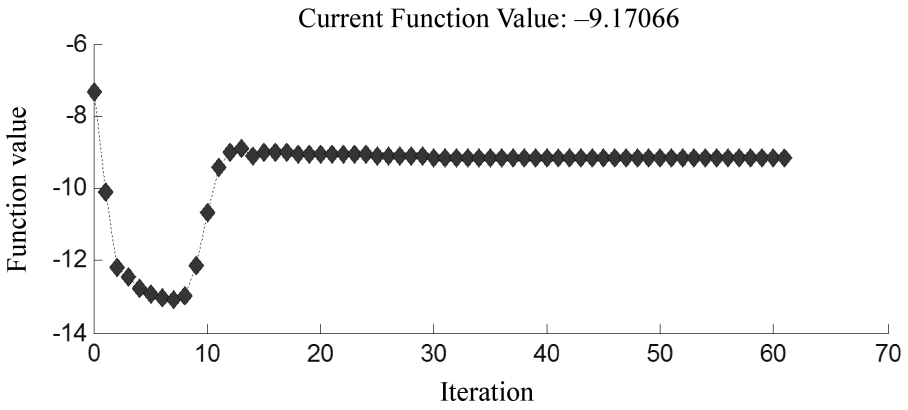

Fig. 4. History of the objective function of the lateral response.

a) original response orbit at the steady state

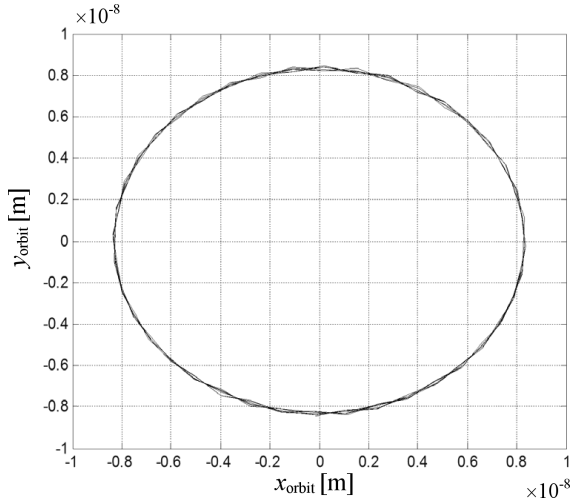

b) optimum response orbit at the steady state

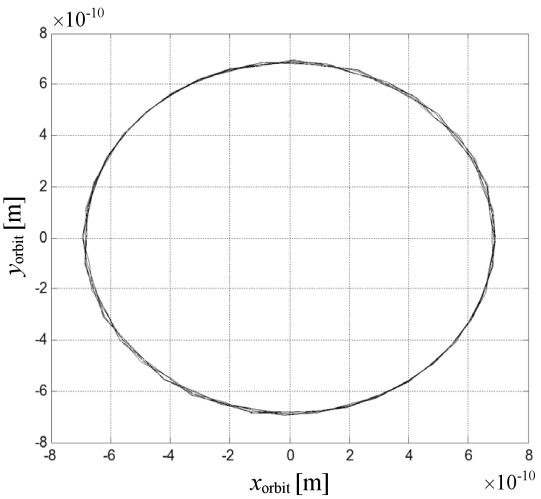

c) original amplitude response

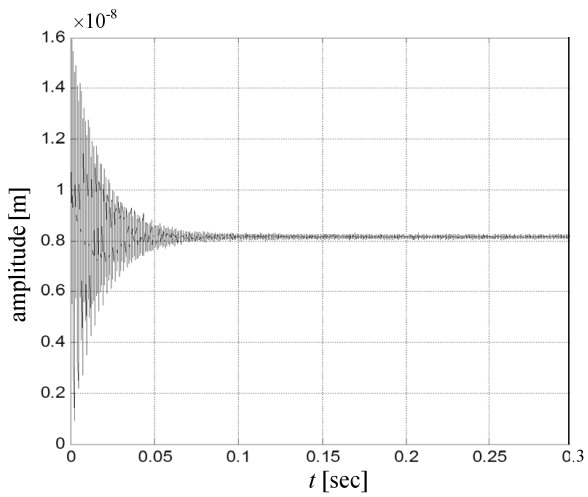

d) optimum amplitude response

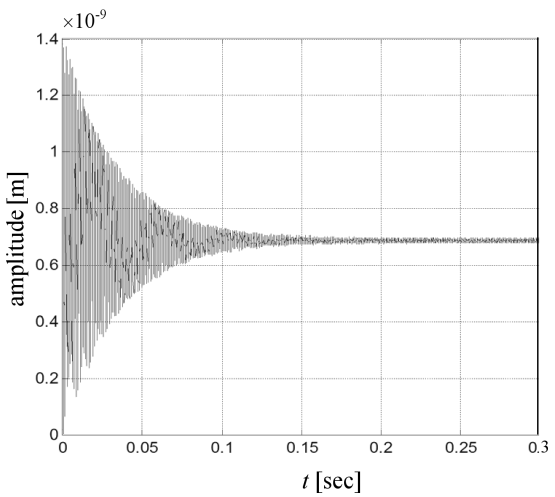

Fig. 5. Original and optimal response orbit and amplitude of the drill point.

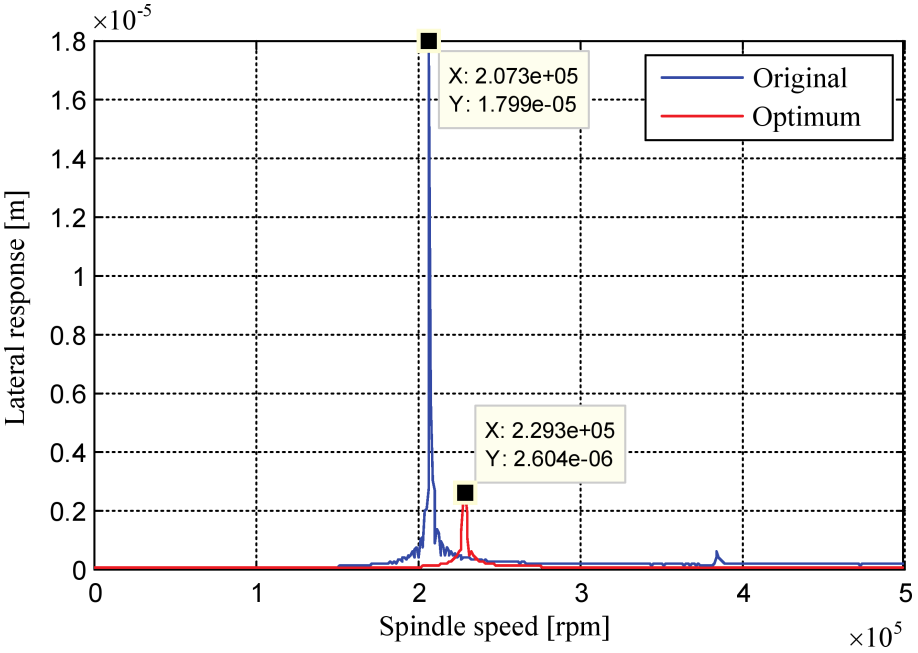

Fig. 6. Lateral responses at the drill point of the original and optimum micro drills.

Figure 5 shows a comparison of the results, which indicates that the optimal response orbit at the steady state is smaller than that of the original one (Figs. 5a and 5b). As shown in Table 4, the percentage error between the optimal and original value of the lateral amplitude response is 91.89%. Figure 6 illustrates the rotational responses of the original and optimal drill. In this optimization run, the first critical speed value moved from 2.073×10^5 r/min to 2.293×10^5 r/min, beyond the operating speed Ω. The lateral amplitude of the optimal micro-drill is smaller than that of the original micro-drill under cutting with a rotation speed of 50 000 r/min. In addition, its value at the first peak is decreased from 1.799×10^{-5} m to 2.604×10^{-6} m.

The sensitivity of design variables to the objective function is analyzed to examine the effects of the variables on the lateral displacement (δ_Ω^x) that corresponds to the vertical axis in Fig. 7.

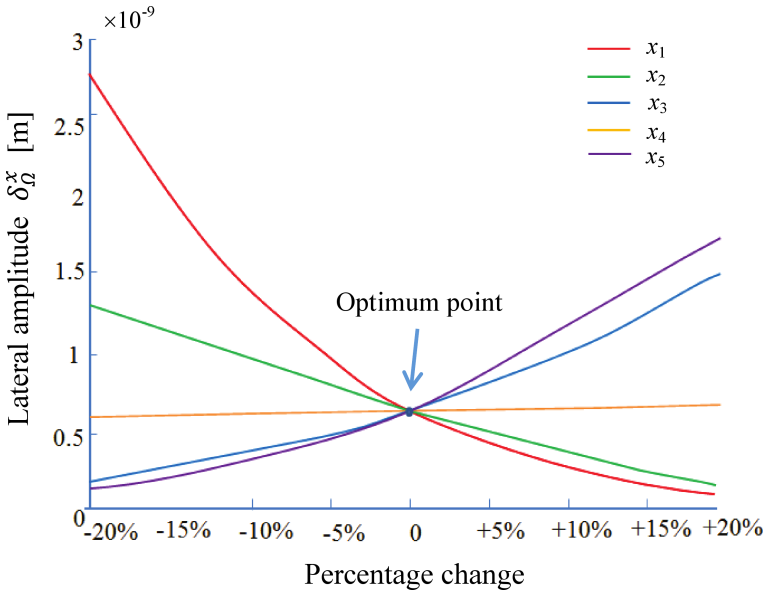

Fig. 7. Chart of local sensitivity curves.

The horizontal axis in Fig. 7 describes the percentage change of the design variables evaluated by Eq. (10).

$$x_i = x_i^{\text{optimum}} \pm 20\% \cdot x_i^{\text{optimum}}; \qquad i = \overline{1,5}, \tag{10}$$

where x_i, and x_i^{optimum} are the design variable and the optimal value of each design variable, respectively. Figure 7 shows the diameter of the lateral amplitude that corresponds to design variable x_1 being reduced, thereby exhibiting the most significant change among other design variables. Hence, design variable x_1 has the greatest influence on the lateral displacement at the drill tip. In this numerical example, owing to the fact that the increase in the cross-sectional diameter increases the stiffness and the enhancement of the diameter lowers the lateral amplitude, the objective function decreases when the percentage change that corresponds to design variable x_1 increases.

4.3. Discussion

In the above numerical example, the micro-drill was optimized at a working speed of 50 000 r/min; however, the drill can work at other speeds if the spindle can provide such speed. Therefore, it is worthy of doing drill optimization at different working speeds. Another numerical example at a speed of 100 000 r/min near the first original critical speed was carried out with the same input parameters. Figures 8 and 9 illustrate the history of the objective function of the lateral response, and optimum response orbit at the steady state, respectively. The values of design variables are $x_1 = 3.2825 \times 10^{-3}$ m, $x_2 = 0.65612 \times 10^{-3}$ m, $x_3 = 0.101 \times 10^{-3}$ m, $x_4 = 6.082 \times 10^{-3}$ m, and $x_5 = 5.422 \times 10^{-3}$ m. Figure 10 summarizes the lateral responses of the original and two optimal drills. The first critical speeds of the original drill, optimal drill at 50 000 r/min, and optimal drill at 100 000 r/min are 2.073×10^5 r/min, 2.293×10^5 r/min, and 2.474×10^5 r/min, respectively. Their peak values are 1.799×10^{-5} m, 2.604×10^{-6} m, and 2.352×10^{-6} m, respectively. Compared to the optimal drill at 50 000 r/min, the critical peak of the optimal drill at 100 000 r/min is further away from the original peak. For the spindle speed of 50 000 r/min, the second optimal drill has smaller amplitude than that of the first optimal drill as shown in Table 5. Therefore, theoretically the second optimal drill is better than the first one at the speed of 50 000 r/min. However, it is challenging to manufacture such drill because the length of the first conical segment ($x_3 = 0.101 \times 10^{-3}$ m)

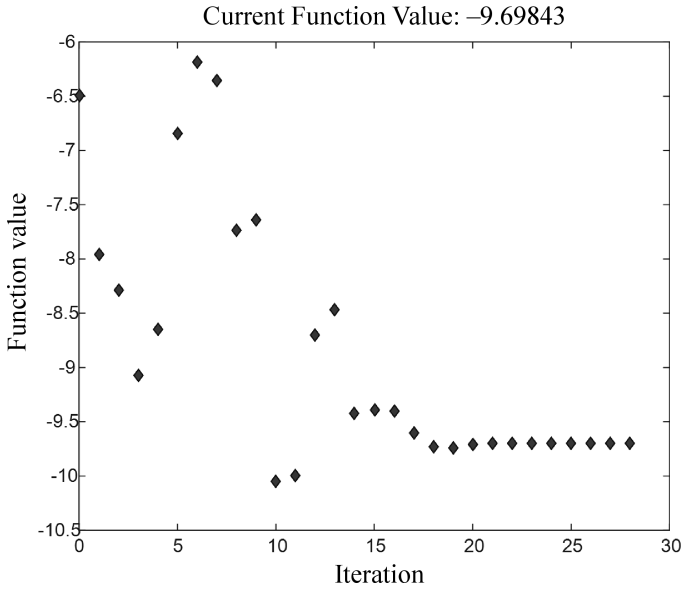

Fig. 8. History of the objective function of the lateral response for the case of 100 000 r/min.

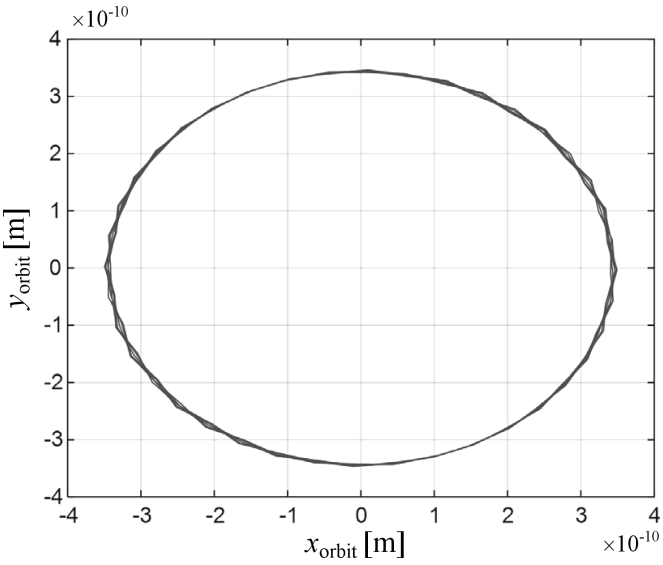

Fig. 9. Optimum steady state orbit at 100 000 r/min.

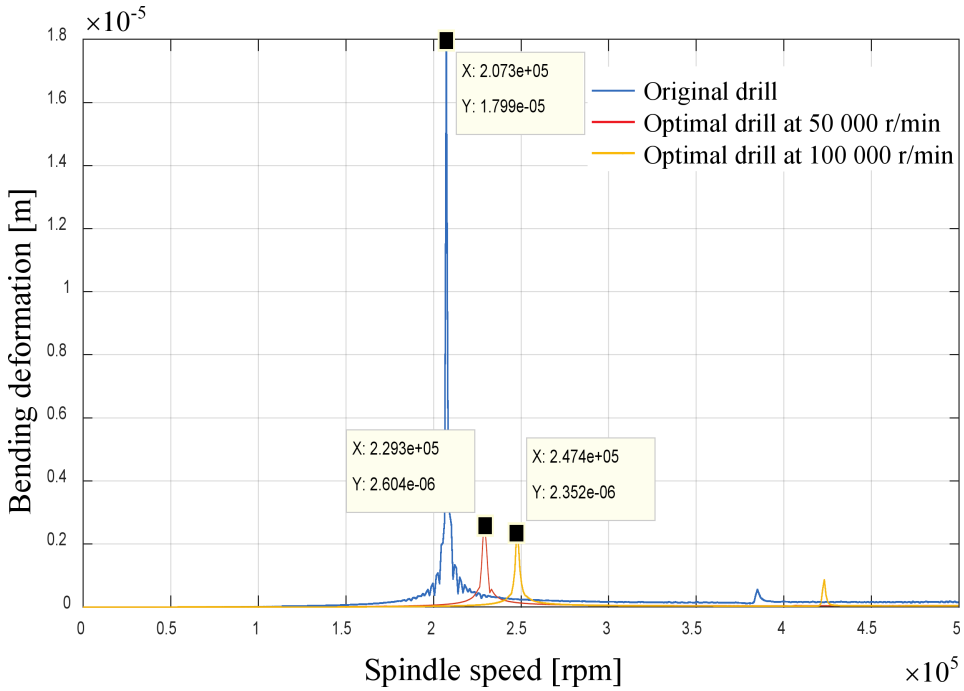

Fig. 10. Lateral responses at the drill point of the original and two optimal micro drills.

is quite small. Hence, with regards to manufacturing capability, the designed drill optimized at 50 000 r/min is considered to be a better choice.

Table 5. Comparison of the original and two optimal drills.

	Original drill at 50 000 r/min	Optimal drill at 50 000 r/min	Optimal drill at 100 000 r/min
Amplitude δ_Ω [m]	8.33×10^{-9}	6.756×10^{-10}	3.502×10^{-10}
The 1st critical speed [r/min]	2.073×10^5	2.293×10^5	2.474×10^5
The 1st peak value [m]	1.799×10^{-5}	2.604×10^{-6}	2.352×10^{-6}

5. Conclusions

The structure optimization of the MDS micro-drill was introduced to improve cutting quality. The results showed that the lateral vibration of the optimal drill decreased by 91.89% at a cutting speed of 50 000 r/min. The first critical speed of the optimal micro-drill exceeds the required operating speed to prevent resonance during the cutting process. A comparison among the design variables, i.e., the diameters and lengths of the drill segments, indicates that the drill shank diameter has the most significant effect on the lateral displacement at the drill tip. The Union MDS micro-drill tool with a 0.1 mm diameter is used as a benchmark, and the performance of drill dynamics can be further improved by our optimum design strategy. The shape of the micro-drill as shown in Fig. 1 is an industrial standard for the PCB industry. The authors assume that the design method can be also applied to other micro-drills of different sizes.

Appendix: shape functions and element matrices

Shape functions of translating displacements:

$$N_{t1} = \frac{1}{1+r}\left[1 - 3\xi^2 + 2\xi^3 + r(1-\xi)\right], \tag{A1}$$

$$N_{t2} = \frac{L}{1+r}\left[\xi - 2\xi^2 + \xi^3 + \frac{r}{2}(\xi - \xi^2)\right], \tag{A2}$$

$$N_{t3} = \frac{1}{1+r}\left[3\xi^3 - 2\xi^2 + r\xi\right], \tag{A3}$$

$$N_{t4} = \frac{L}{1+r}\left[-\xi^2 + \xi^3 + \frac{r}{2}(-\xi + \xi^2)\right]. \tag{A4}$$

Shape functions of rotational displacements:

$$N_{r1} = \frac{1}{(1+r)L}(-6\xi + 6\xi^2), \tag{A5}$$

$$N_{r2} = \frac{1}{1+r}\left[1 - 4\xi + 3\xi^2 + r(1-\xi)\right], \tag{A6}$$

$$N_{r3} = \frac{1}{(1+r)L}(6\xi - 6\xi^2), \tag{A7}$$

$$N_{r4} = \frac{1}{1+r}(-2\xi + 3\xi^2 + r\xi). \tag{A8}$$

Shape functions of torsional displacements:

$$N_{\varphi 1} = 1 - \xi, \tag{A9}$$

$$N_{\varphi 2} = \xi. \tag{A10}$$

Composed shape functions:

$$[N^e] = \begin{bmatrix} N_{t1} & 0 & N_{t2} & 0 & 0 & N_{t3} & 0 & N_{t4} & 0 & 0 \\ 0 & N_{t1} & 0 & -N_{t2} & 0 & 0 & N_{t3} & 0 & -N_{t4} & 0 \\ N_{r1} & 0 & N_{r2} & 0 & 0 & N_{r3} & 0 & N_{r4} & 0 & 0 \\ 0 & -N_{r1} & 0 & N_{r2} & 0 & 0 & -N_{r3} & 0 & N_{r4} & 0 \\ 0 & 0 & 0 & 0 & N_{\varphi 1} & 0 & 0 & 0 & 0 & N_{\varphi 1} \end{bmatrix}, \tag{A11}$$

$$\xi = \frac{z}{L}, \tag{A12}$$

$$r = \frac{6E(I_u + I_v)}{k_s G A L^2}. \tag{A13}$$

References

[1] J. Agapiou, E. Rivin, C. Xie. Toolholder/spindle interfaces for CNC machine tools. *CIRP Annals – Manufacturing Technology*, **44**(1): 383–387, 1995.

[2] M.A. Alfares, A.A. Elsharkawy. Effects of axial preloading of angular contact ball bearings on the dynamics of a grinding machine spindle system. *J. Mater. Process. Technol.*, **136**(1): 48–59, 2003.

[3] J.R. Baker, K.E. Rouch. Use of finite element structural models in analyzing machine tool chatter. *Finite Elem. Anal. Des.*, **38**(11): 1029–1046, 2002.

[4] B.K. Choi, B.S. Yang. Multiobjective optimum design of rotor-bearing systems with dynamic constraints using immune-genetic algorithm. *J. Eng. for Gas Turbines and Power*, **123**(1): 78–81, 2001.

[5] B.G. Choi, B.S. Yang. Optimum shape design of rotor shafts using genetic algorithm. *J. Vib. Control*, **6**(2): 207–222, 2000.

[6] R.P.H. Faassen, N. Van de Wouw, J.A.J. Oosterling, H. Nijmeijer. Prediction of regenerative chatter by modelling and analysis of high-speed milling. *Int. J. Mach. Tools Manuf.*, **43**(14): 1437–1446, 2003.

[7] V. Gagnol, B.C. Bouzgarrou, P. Ray, C. Barra. Stability-based spindle design optimization. *J. Manuf. Sci. Eng.*, **129**(2): 407–415, 2007.

[8] I. Griva, S. Nash, A. Sofer. *Linear and Nonlinear Optimization*. The Society for Industrial and Applied Mathematics, Siam, Philadelphia, 2009.

[9] M.Y. He, M. Kiemb, A.L. Tits, A. Greenfield, V. Sahasrabudhe. Constraint-reduced interior-point optimization for model predictive rotorcraft control. *American Control Conference*, 2088–2094, IEEE, 2010.

[10] Y.H. Kim, A. Tan, B.S. Yang, W.C. Kim, B.K. Choi, Y.S. An. Optimum shape design of rotating shaft by ESO method. *J. Mech. Sci. and Tech.*, **21**(7): 1039–1047, 2007.

[11] A.C. Lee, C.S. Liu. Analysis of chatter vibration in the end milling process. *Int. J. Mach. Tools Manuf.*, **31**(4): 471–479, 1991.

[12] A.C. Lee, C.S. Liu, S.T. Chiang. Analysis of chatter vibration in a cutter-workpiece system. *Int. J. Mach. Tools Manuf.*, **31**(2): 221–234, 1991.

[13] A.C. Lee, T.D. Hoang. Coupled lateral and torsional vibrations of the micro-drilling spindle systems. *Int. J. Adv. Manuf. Technol.*, **87**(5): 2063–2079, 2016.

[14] N. Olgac, M. Hosek. A new perspective and analysis for regenerative machine tool chatter. *Int. J. Mach. Tools Manuf.,* **38**(7): 783–798, 1998.

[15] A.O. Pugachev. Application of gradient-based optimization methods for a rotor system with static stress, natural frequency, and harmonic response constraints. *Struct. Multidiscip. Optim.*, **47**(6): 951–962, 2013.

[16] P. Pardalos, J.R. Birge, D.Z. Du, C.A. Floudas, J. Mockus, H.D. Sherali, G. Stavroulakis. *Nonconvex Optimization and Its Applications*, Springer, 1994.

[17] S.S. Rao, E.L. Mulkay. Engineering design optimization using interior-point algorithms. *AIAAJ*, **38**(11): 2127–2132, 2000.

[18] S. Smith, T.P. Jacobs, J. Halley. The effects of drawbar force on metal removal rate in milling. *CIRP Ann, Technol.*, **48**(1): 293–296, 1999.

[19] Y.C. Shin. Bearing nonlinearity and stability analysis in high speed machining. *J. Eng. Ind. ASME*, **114**(1): 23–30, 1992.

[20] H. Saruhan. Optimum design of rotor-bearing system stability performance comparing an evolutionary algorithm versus a conventional method. *Int. J. Mech. Sci.*, **48**(12): 1341–1351, 2006.

[21] W.R. Wang, C.N. Chang. Dynamic analysis and design of a machine tool spindle-bearing system. *J. Vib. Acoust.*, **116**(3): 280–285, 1994.

[22] B.S. Yang, S.P. Choi, Y.C. Kim. Vibration reduction optimum design of a steam-turbine rotor-bearing system using a hybrid genetic algorithm. *Struct. Multidiscip. Optim.*, **30**(1): 43–53, 2005.